

De Broglie - Bohm Cycles. Free Relativistic One-Half Particles

To my beloved Isabel

Olivier Piguet*

June 6, 2023

Abstract

In the de Broglie-Bohm quantum theory, particles describe trajectories determined by the flux associated with their wave function. These trajectories are studied here for relativistic spin-one-half particles. Based in explicit numerical calculations for the case of a massless particle in dimension three space-time, it is shown that if the wave function is an eigenfunction of the total angular momentum, the trajectories – here called “de Broglie-Bohm cycles” – begin as circles of slowly increasing radius until a transition time at which they tend to follow straight lines. Arrival times at some detector, as well as their probability distribution are calculated, too. The chosen energy and momentum parameters are of the orders of magnitude met in graphene’s physics.

Keywords: de Broglie-Bohm; Quantum Mechanics; Transport properties; Graphene.

1 Introduction

Since its beginning in the first decades of XXth century [1]-[7] Quantum Mechanics and its extension in the form of Quantum Field Theory led to an accurate description of atomic and subatomic phenomena, confirmed in an extraordinarily precise way by countless experiments. However, there is no such broad consensus about its interpretation. Various ones are present in the literature, such as the Copenhagen [8], the Many-Worlds [9], the Relational [10] or the de Broglie-Bohm (dBB) one. We will deal here with the latter interpretation, first proposed by Louis de Broglie [4] as the “Pilot Wave Theory”, later on formulated by David Bohm [11, 12]

*Praça Graccho Cardoso, 76/504, 45015-180 Aracaju, SE, Brazil, E-mail: opiguet@yahoo.com

as the "Ontological Interpretation of Quantum Theory" and finally, critically defended by John Bell in a series of papers reproduced in [13]. This interpretation of Quantum Mechanics differs essentially from the largely more widespread Copenhagen interpretation by taking particle trajectories as elements of reality, *i.e.*, a particle really follows a trajectory, the latter being defined by "guiding conditions" first proposed by de Broglie. A probabilistic interpretation is maintained, but now in the sense of classical statistical mechanics. The trajectory followed by a particle is fully defined by giving boundary conditions such as, *e.g.*, the coordinates of its initial position. The probability distribution of the particle following a particular trajectory is then given by the value of the squared modulus of the wave function taken at the initial time and position. Since this statistical distribution is equal to the "usual" (Copenhagen) quantum probability distribution and in particular satisfies the same conservation conditions, mean values of observables evolve identically in both interpretations of Quantum Mechanics.

The first aim of the present paper is to introduce the reader to the dBB theory by treating simple physical examples. Since the main peculiarity of this interpretation is the factual existence of trajectories, some effort will be made in the study of these trajectories and their properties.

The dBB trajectories we will calculate are those of a relativistic¹, massive or massless, spin one half particle in dimension 3 space-time. Its quantum state will be supposed to be described by an eigenfunction of the total angular momentum J defined relatively to some space point². Stationary as well as packets of stationary wave functions will be considered. The main result for the latter is that the dBB trajectories consist of an initial phase of quasi circles whose radius increases till a critical time at which the trajectory begins tending to a straight line – the straight line expected for a classical particle with definite angular momentum.

The concept of trajectory also allows for a natural definition of the arrival time at a detector, of a particle prepared in some initial state[14, 15, 16]³. Calculations of such arrival times will be presented, together with their probability distributions.

The paper begins in Section 2 with an introduction to the dBB formalism and in Section 3 for its application to the relativistic spin one half particle described by the Dirac equation. Numerical computations of dBB trajectories and arrival times for electrons in the context of graphene's transport properties are presented in Section 3.3. Final considerations are given in the Conclusion Section.

Most analytic and numerical calculations are made with the help of the software Mathematica [21].

¹Only the theory of a single particle is considered here. See [17, 18, 19] for a discussion of the N -particle relativistic case.

²See [20] for the calculation of such states in the case of the non-relativistic free particle.

³See [15, 16] for an interesting proposal for an experiment.

2 Summary of the de Broglie-Bohm theory

In the "usual" (*i.e.*, Copenhagen) interpretation of Quantum Mechanics [8], the dynamics of a physical system constituted of a single particle is described, in the Schrödinger picture, by a wave equation

$$i\hbar \frac{\partial \psi(\mathbf{x}, t)}{\partial t} = \hat{H} \psi(\mathbf{x}, t), \quad (2.1)$$

where \hat{H} is a self-adjoint partial derivative operator acting on a N -components wave function

$$\psi(\mathbf{x}, t) = \begin{pmatrix} \psi_1(\mathbf{x}, t) \\ \dots \\ \psi_N(\mathbf{x}, t) \end{pmatrix}, \quad (2.2)$$

belonging to a Hilbert space, with scalar product and norm defined by⁴

$$\langle \psi | \Phi \rangle = \int_{\mathbb{R}^d} d^d x \psi^\dagger(\mathbf{x}, t) \phi(\mathbf{x}, t) = \int_{\mathbb{R}^d} d^d x \sum_{\alpha=1}^N (\psi_\alpha^* \phi_\alpha)(\mathbf{x}, t), \quad \|\psi\| = \langle \psi | \psi \rangle^{\frac{1}{2}}. \quad (2.3)$$

$\mathbf{x} = (x^i, i = 1, \dots, d)$ are the space coordinates, d the space dimension and $\dagger, *$ denote the hermitian and complex conjugate, respectively. The number of components, N , depends on the particle's spin and on the space dimension d . *E.g.*, $N = 1$ for a scalar (spin 0) particle, $N = 2$ for a non-relativistic particle of spin 1/2 in any dimension, $N = 2$ for a relativistic particle of spin 1/2 in 2 dimensions, $N = 4$ for the same in 3 dimensions, *etc.* [22].

The wave equation (2.1) implies the existence of a non-negative density

$$\rho(\mathbf{x}, t) = \psi^\dagger(\mathbf{x}, t) \psi(\mathbf{x}, t), \quad (2.4)$$

and an associate d-current density⁵ $\mathbf{j}(\mathbf{x}, t)$ obeying a continuity equation

$$\partial_t \rho + \nabla \cdot \mathbf{j} = 0, \quad (2.5)$$

which assures the constancy of the norm defined in (2.3). Normalizing the norm to 1, one interprets ρ as a probability density and \mathbf{j} as a probability flux.

In the Copenhagen theory, the state of the system is completely characterized by the wave function ψ , solution of the wave equation (2.1), with an arbitrarily given initial wave function $\psi(\mathbf{x}, 0) = \psi_0(\mathbf{x})$. The de Broglie-Bohm (dBB) theory completes the characterization of the state of the system (the particle, here) by postulating the existence of a trajectory, determined by the de Broglie "guidance conditions" [4] for the particle's velocity

$$\mathbf{v}(\mathbf{x}, t) = \mathbf{j}(\mathbf{x}, t) / \rho(\mathbf{x}, t), \quad (2.6)$$

⁴This holds *e.g.*, for a non-relativistic particle in general, or a spin 1/2 relativistic one. We do not consider here cases such as the relativistic spin zero particle described by the Klein-Gordon equation.

⁵Its explicit form will be given below for the cases studied there.

the dBB trajectory $\mathbf{x}_B(\mathbf{x}_0, t)$ being then a solution of the set of differential of equations

$$\frac{\partial \mathbf{x}_B(\mathbf{x}_0, t)}{\partial t} = \mathbf{v}(\mathbf{x}_B(\mathbf{x}_0, t), t), \quad (2.7)$$

with an arbitrarily given initial position $\mathbf{x}_B(\mathbf{x}_0, 0) = \mathbf{x}_0$. In other words, the possible trajectories are the integral lines of the dBB vector field $\mathbf{v}(\mathbf{x}, t)$, labelled by their initial position \mathbf{x}_0 . Since the flux \mathbf{j} and the density ρ turn out to be both” bilinear in ψ and ψ^\dagger (see later on), the dBB trajectories do not depend on the “intensity” of the wave function, but only on its “form”.

Recall that, in the quantum probabilistic interpretation of Copenhagen, the density ρ represents the probability of experimentally finding the particle at a given place at a given time. On the other hand, the dBB theory treats this density in a more “classical statistical mechanics” way: Trajectories “really happen”, and their probability distribution, which amounts to the probability distribution of their initial positions \mathbf{x}_0 , is given [23] by the density $\rho(\mathbf{x}_0, 0)$. The latter represents our lack of knowledge of the precise initial position. Thanks to the continuity equation (2.5), the probability for the particle being inside a co-moving volume⁶ $V(t)$ is constant in time, which sustains this statistical interpretation, called “thermal equilibrium” in the literature [23].

Such a formulation is called a theory with “hidden variables”, the hidden variables of the present one being, *e.g.*, the components of the initial position \mathbf{x}_0 .

A heuristic justification for the guiding condition (2.6) may be found in analogy with fluid mechanics, considering ρ and \mathbf{v} as the fluid mass density and velocity field, respectively. With $\mathbf{j} = \rho\mathbf{v}$, Eq. (2.5) has the form of the continuity equation expressing the conservation of the fluid mass.

To summarize, the dBB theory proposes the existence of:

1. A wave function or ”guidance field” (2.2), solution of the Schrödinger-like wave equation (2.1).
2. A statistical ensemble of particle’s trajectories $\mathbf{x}_B(\mathbf{x}_0, t)$ as the integral lines of the dBB vector field (2.6), solutions of the differential equations (2.7) parametrized by the value of the initial position.

All considerations made in this subsection generalize easily to systems of N particles, \mathbf{x} denoting a point of the $d \times N$ dimensional configuration space⁷.

⁶*I.e.*, a volume whose boundary points move along the dBB trajectories.

⁷At least in the non-relativistic case. See footnote 1.

3 Free relativistic spin one half particle in 3-dimensional space-time

3.1 Dirac equation

A free, spin 1/2 relativistic particle of mass m in 3-dimensional space-time is described in the usual theory by a 2-components spinor wave function

$$\psi(x) = \begin{pmatrix} \psi_1(x) \\ \psi_2(x) \end{pmatrix}, \quad (3.1)$$

solution of the free Dirac equation

$$i\hbar c \gamma^\mu \partial_\mu \psi(x) - mc^2 \psi(x) = 0, \quad (3.2)$$

where $x = (x^\mu, \mu = 0, 1, 2)$ are the space-time coordinates space-time, whose metric is $\eta_{\mu\nu} = \text{diag}(1, -1, -1)$. The Dirac matrices obey the anti-commutation rules $\{\gamma^\mu, \gamma^\nu\} = 2\eta_{\mu\nu}$. Our choice for them is given in Appendix A. c , \hbar are the speed of light and the reduced Planck constant, respectively. The Dirac equation may be cast in the form⁸ of (2.1):

$$i\hbar \frac{\partial \psi(\mathbf{x}, t)}{\partial t} = \hat{H} \psi(\mathbf{x}, t), \quad (3.3)$$

with

$$\hat{H} = -i\hbar c \alpha^i \partial_i + mc^2 \beta, \quad (3.4)$$

with $\alpha^i = \gamma^0 \gamma^i$ and $\beta = \gamma^0$ (see Appendix A). The density and the flux obeying the continuity equation (2.5) are given by

$$\rho = \psi^\dagger \psi, \quad j^i = c \psi^\dagger \alpha^i \psi. \quad (3.5)$$

The theory is relativistic: $c\rho$ and j^i are the time and space components of the space-time 3-vector $j^\mu = \bar{\psi} \gamma^\mu \psi$, and the continuity equation reads $\partial_\mu j^\mu = 0$.

Another relativistic object is the scalar density

$$\sigma(\mathbf{x}, t) = \frac{1}{2} \bar{\psi} \psi = \frac{1}{2} \psi^\dagger \beta \psi. \quad (3.6)$$

j^μ and σ fulfil the identity

$$j^\mu j_\mu = 4\sigma^2, \quad (3.7)$$

consequence of the Pauli matrices identity

$$\sum_{i=1}^3 \sigma_{\alpha\beta}^i \sigma_{\gamma\delta}^i = 2\delta_{\alpha\delta} \delta_{\beta\gamma} - \delta_{\alpha\beta} \delta_{\gamma\delta}. \quad (3.8)$$

⁸In fact Dirac's original form, reduced to 3 space-time dimensions.

Let us go now to the dBB theory. The identity (3.7) allows one to define the time-like 3-velocity field'

$$u^\mu = \frac{j^\mu}{2|\sigma|}, \quad u^\mu u_\mu = 1, \quad u^0 > 0. \quad (3.9)$$

The relativistic form of the dBB guidance equation (2.7) then reads⁹

$$\frac{dx^\mu(\lambda)}{d\lambda} = u^\mu(x(\lambda)), \quad (3.10)$$

with λ as curve's parameter. This equation is equivalent to (2.7) and defines the space-time trajectories of the particle. The more practical non-covariant formalism based on Eqs. (2.7) and (3.3) will be used in the following.

3.2 Eigenstates of the angular momentum and of the energy

We will look for the solutions of the Dirac equation which are eigenfunctions of the total angular momentum and Hamiltonian operators. It will be useful to work in polar coordinates r, ϕ :

$$x = r \cos \phi, \quad y = r \sin \phi.$$

In these coordinates, the Hamiltonian operator (3.4) reads

$$\hat{H} = -i\hbar c \left((\alpha^1 \cos \phi + \alpha^2 \sin \phi) \partial_r + \frac{1}{r} (\alpha^2 \cos \phi - \alpha^1 \sin \phi) \partial_\phi \right) + mc^2 \beta. \quad (3.11)$$

One easily checks, using the algebra of the Pauli matrices, that the total angular momentum operator with respect to the origin, which has a single component in the two-dimensional space's case,

$$\hat{J} = \hat{L} + \hat{S}, \quad \text{with} \quad \hat{L} = -i\hbar \partial_\phi, \quad \hat{S} = \frac{\hbar}{2} \beta, \quad (3.12)$$

commutes with the Hamiltonian operator. Spinor eigenfunctions of \hat{J} with eigenvalue j are readily found to be of the form

$$\psi(r, \phi, t) = \begin{pmatrix} e^{i(j-\frac{1}{2})\phi} f_1(r, t), \\ e^{i(j+\frac{1}{2})\phi} f_2(r, t) \end{pmatrix}. \quad (3.13)$$

One directly sees that the requirement of the wave function to be single-valued requires j to be half-integer. With the result (3.13), solving the Dirac equation (3.2) amounts to solving the two radial equations for the functions $f_1(r, t)$ and $f_2(r, t)$:

$$\begin{aligned} i\hbar \left(r (\partial_t f_1 + c \partial_r f_2) + c(j + \frac{1}{2}) f_2 \right) - mc^2 r f_1 &= 0, \\ i\hbar \left(r (\partial_t f_2 + c \partial_r f_1) - c(j - \frac{1}{2}) f_1 \right) + mc^2 r f_2 &= 0. \end{aligned} \quad (3.14)$$

⁹The present discussion is the reduction to 3-dimensional space-time of the one made by [24, 17] in 4 dimensions.

In terms of the radial functions f_α , the probability density ρ and the flux \mathbf{j} read:

$$\begin{aligned}\rho(r, t) &= |f_1(r, t)|^2 + |f_2(r, t)|^2, \\ j_x(r, \phi, t) &= c \left(e^{i\phi} f_1^*(r, t) f_2(r, t) + e^{-i\phi} f_2^*(r, t) f_1(r, t) \right), \\ j_y(r, \phi, t) &= ic \left(-e^{i\phi} f_1^*(r, t) f_2(r, t) + e^{-i\phi} f_2^*(r, t) f_1(r, t) \right).\end{aligned}\tag{3.15}$$

The density ρ , as well as the radial and azimuthal components of the flux \mathbf{j} ,

$$\begin{aligned}j_r(r, t) &= \cos \phi j_x(r, \phi, t) + \sin \phi j_y(r, \phi, t) = c (f_1^*(r, t) f_2(r, t) + f_2^*(r, t) f_1(r, t)), \\ j_\phi(r, t) &= -\sin \phi j_x(r, \phi, t) + \cos \phi j_y(r, \phi, t) = ic (-f_1^*(r, t) f_2(r, t) + f_2^*(r, t) f_1(r, t)),\end{aligned}\tag{3.16}$$

turn out to be independent of the angular coordinate.

3.2.1 Stationary solutions:

Since the Hamiltonian (3.11) and the total angular momentum (3.12) commute, we can impose the stationarity condition

$$\hat{H}\psi = \hbar\omega_p \psi.\tag{3.17}$$

Thus the radial wave functions $f_\alpha(r, t)$ take the form

$$f_\alpha^{p, \text{stat}}(r, t) = e^{-i\omega_p t} h_\alpha^{p, \text{stat}}(r), \quad \alpha = 1, 2,\tag{3.18}$$

$\hbar\omega_p$ being the energy of the stationary state. This leads to a pair of equations for the function $h_\alpha^{p, \text{stat}}(r)$, derived from (3.14) by substituting $i\partial_t$ by ω_p . The general solution of these equations is a superposition of the Bessel functions of the first and second kind, $J_{j\pm 1/2}(pr/\hbar)$ and $Y_{j\pm 1/2}(pr/\hbar)$, with p a function of ω_p defined as the positive solution for p of

$$\omega_p = \frac{1}{\hbar} \sqrt{m^2 c^4 + p^2 c^2}.\tag{3.19}$$

Square integrability of the wave function at $r = 0$ leads us to discard the solutions involving $Y_{j\pm 1/2}$ because of the latter's singularity at the origin (see (B.3) in Appendix B). The regular solution thus is

$$h_1^{p, \text{stat}}(r) = icp J_{j-1/2}(pr/\hbar), \quad h_2^{p, \text{stat}}(r) = -(\hbar\omega_p - mc^2) J_{j+1/2}(pr/\hbar).\tag{3.20}$$

The general stationary solution of the Dirac equation for angular momentum eigenstates, non-singular at the origin, then reads

$$\begin{aligned}\psi^{p, \text{stat}}(r, \phi, t) &= \begin{pmatrix} e^{i(j-\frac{1}{2})\phi} f_1^{p, \text{stat}}(r, t), \\ e^{i(j+\frac{1}{2})\phi} f_2^{p, \text{stat}}(r, t) \end{pmatrix} \\ &= e^{-i\omega_p t} \begin{pmatrix} icp e^{i(j-1/2)\phi} J_{j-1/2}(pr/\hbar), \\ -(\hbar\omega_p - mc^2) e^{i(j+1/2)\phi} J_{j+1/2}(pr/\hbar) \end{pmatrix},\end{aligned}\tag{3.21}$$

with ω_p given by (3.19). These spinors form a basis for the solutions of the Dirac equation, however an improper one since they are not square integrable due to the asymptotic behaviour of the Bessel functions shown in (B.4) of Appendix B.

We can nevertheless apply the dBB guidance principle, expressed in Eqs, (2.6) and (2.7), to such a basis element. From the result (3.21) we can compute explicitly the density ρ given in (3.15):

$$\rho^{p,\text{stat}}(r) = c^2 p^2 J_{j-1/2}^2(pr/\hbar) + (\hbar\omega_p - mc^2)^2 J_{j+1/2}^2(pr/\hbar), \quad (3.22)$$

as well as the flux components (3.16) which, divided through ρ according to the dBB condition, yields the radial and azimuthal components of the velocity vector field:

$$\begin{aligned} v_r^{p,\text{stat}}(r) &= 0 \\ v_\phi^{p,\text{stat}}(r) &= 2c \frac{cp(\hbar\omega_p - mc^2)J_{j-1/2}(pr/\hbar)J_{j+1/2}(pr/\hbar)}{(cp)^2 J_{j-1/2}^2(pr/\hbar) + (\hbar\omega_p - mc^2)^2 J_{j+1/2}^2(pr/\hbar)}. \end{aligned} \quad (3.23)$$

Obviously all these expressions are time independent due to the stationarity condition. One sees that the radial component of the velocity field is vanishing and that its azimuthal component does not depend on the polar angle. Thus the dBB trajectories of the particle, defined as the integral curves of the velocity vector field, are circles of radius r centred at the origin travelled at a constant velocity v_ϕ and whose radius dependent value is bounded by c , in the massive as well as in the massless case. In all cases the bound c is effectively reached, for a discrete set of values of the radius. Fig. 1 in Subsection 3.3 shows a typical behaviour of the azimuthal velocity $v_\phi^{p,\text{stat}}(r)$ in the massless particle's case.

One may observe that, in the massless case, in which $\hbar\omega_p = pc$, changing the sign of the total angular momentum implies a change of sign of the velocity field: $v_\phi^{p,\text{stat}}(r) \rightarrow -v_\phi^{p,\text{stat}}(r)$, hence of the orientation of the trajectories. However this does not hold for the massive case, and also not for the more general wave packets examined in Subsection (3.2.2).

3.2.2 Gaussian wave packet

The general solution of the Dirac equation for angular momentum eigenstates, non-singular at the origin, reads

$$\psi(\mathbf{x}, t) = \int_0^\infty dp a(p) \psi^{p,\text{stat}}(\mathbf{x}, t), \quad (3.24)$$

where $\psi^{p,\text{stat}}$ is the stationary solution (3.21) of energy¹⁰ $\hbar\omega_p$ given by (3.19), and the amplitude $a(p)$ is an arbitrary complex function, but constrained by the requirement of $\psi(\mathbf{x}, t)$ to be a square integrable function of \mathbf{x} .

The angular momentum eigenstates we will consider in the following are described by the

¹⁰We restrict to positive energy contributions.

spinor wave functions of the form (3.24), with $a(p)$ the Gaussian amplitude

$$a(p) = \sqrt{p} e^{-\frac{(p-p_0)^2}{2\Sigma^2}}. \quad (3.25)$$

Here and in the rest of this paper we consider only positive energy solutions of the Dirac equations.

3.2.3 Mean values

We recall that mean values of observables obtained from the dBB or from the Copenhagen theory coincide.

The wave functions (3.24) are normalizable and we can calculate the square norm $\|\psi\|^2$ in the following way:

$$\|\psi\|^2 = \int_0^{2\pi} d\phi \int_0^\infty dr r \rho(r, t),$$

with $\rho(r, t)$ the density (3.5). From (3.24) we get

$$\begin{aligned} \|\psi\|^2 &= 2\pi \int_0^\infty dr r \int_0^\infty dp \int_0^\infty dp' a(p)a(p') \sum_{\alpha=1}^2 f_\alpha^{p, \text{stat}}(r, t)^* f_\alpha^{p', \text{stat}}(r, t) \\ &= 2\pi \int_0^\infty dp \int_0^\infty dp' a(p)a(p') e^{i(\omega_p - \omega_{p'})} \int_0^\infty dr r \\ &\quad ((mc^2 + \hbar\omega_p)(mc^2 + \hbar\omega_{p'}) J_{j-1/2}(pr/\hbar) J_{j-1/2}(p'r/\hbar) + \hbar^2 pp' J_{j+1/2}(pr/\hbar) J_{j+1/2}(p'r/\hbar)). \end{aligned}$$

From (3.25) and the completeness identity [25] for the Bessel functions:

$$\int_0^\infty dr r J_l(kr) J_l(k'r) = \frac{1}{k} \delta(k - k'),$$

one gets

$$\|\psi\|^2 = 2\pi \hbar^2 \int_0^\infty dp \frac{1}{p} a^2(p) (c^2 p^2 + (\hbar\omega_p - mc^2)^2). \quad (3.26)$$

In the same way one establishes expressions for the mean energy:

$$\langle E \rangle = \int_0^{2\pi} d\phi \int_0^\infty dr r \psi^\dagger(r, \phi, t) \hat{H} \psi(r, \phi, t) / \|\psi\|^2,$$

where \hat{H} is the Hamiltonian operator (3.4), and for the standard energy deviation

$$\Delta E = \sqrt{\langle E^2 \rangle - \langle E \rangle^2}.$$

The result is

$$\begin{aligned} \langle E \rangle &= \frac{2\pi \hbar^2}{\|\psi\|^2} \int_0^\infty dp \frac{1}{p} a^2(p) (c^2 p^2 + (\hbar\omega_p - mc^2)^2) \hbar\omega_p, \\ \Delta E &= \left(\frac{2\pi \hbar^2}{\|\psi\|^2} \int_0^\infty dp \frac{1}{p} a^2(p) (c^2 p^2 + (\hbar\omega_p - mc^2)^2) (\hbar\omega_p)^2 - \langle E \rangle^2 \right)^{\frac{1}{2}}. \end{aligned} \quad (3.27)$$

Finally, a computation of the mean value of the spin operator \hat{S} defined by (3.12) yields

$$\langle S \rangle = \frac{\pi \hbar^3}{\|\psi\|^2} \int_0^\infty dp \frac{1}{p} a^2(p) (-c^2 p^2 + (\hbar \omega_p - mc^2)^2). \quad (3.28)$$

Substituting $\|\psi\|^2$ in the denominator by its expression (3.26), one sees that this mean value obeys the bounds $-\hbar/2 < \langle S \rangle < \hbar/2$.

All these integrals can be computed analytically in the massless case for the amplitude given by (3.25). One then gets, for $m = 0$,

$$\begin{aligned} \|\psi\|^2 &= \pi \hbar^2 c^2 \Sigma^3 \left(\sqrt{\pi} (1 + 2z^2) (1 + \operatorname{erf}(z)) + 2z e^{-z^2} \right), \\ \langle E \rangle &= cp_0 \frac{\sqrt{\pi} z (3 + 2z^2) (1 + \operatorname{erf}(z)) + 2(1 + z^2) e^{-z^2}}{z (\sqrt{\pi} (1 + 2z^2) (1 + \operatorname{erf}(z)) + 2z e^{-z^2})}, \end{aligned} \quad (3.29)$$

$$\Delta E = cp_0 \sqrt{\frac{\pi(3 + 4z^4)(1 + \operatorname{erf}(z))^2 + 8\sqrt{\pi}z(-1 + z^2)(1 + \operatorname{erf}(z))e^{-z^2} + 4(-2 + z^2)e^{-2z^2}}{2z^2(\pi(1 + 2z^2)^2(1 + \operatorname{erf}(z))^2 + 4\sqrt{\pi}z(1 + 2z^2)(1 + \operatorname{erf}(z))e^{-z^2} + 4z^2e^{-2z^2})}} \quad (3.30)$$

where we have set

$$z = \frac{p_0}{\Sigma}, \quad (3.31)$$

and $\operatorname{erf}(z)$ is the error function [26].

Finally, the mean spin is null in this massless case:

$$\langle S \rangle = 0, \quad (3.32)$$

which implies $\langle L \rangle = \hbar j$ for the orbital angular momentum since the states considered are eigenstates of the total angular momentum with eigenvalue $\hbar j$. Associated to this mean orbital angular momentum, we can define an *L-radius*

$$r_L = \frac{\langle L \rangle}{\langle p \rangle} = \frac{c \hbar j}{\langle E \rangle}, \quad (3.33)$$

where $\langle p \rangle$ is the mean value of the momentum p , equal to $\langle E \rangle / c$ in the present massless case. This definition mimics the classical relation between angular momentum and radius for a uniform circular motion.

As one may expect, in the case of a very narrow width of the amplitude (3.25), *i.e.*, $z \gg 1$, the energy and the energy uncertainty approximate to the values

$$\langle E \rangle \simeq cp_0, \quad \Delta E \simeq \frac{c}{\sqrt{2}} \Sigma. \quad (3.34)$$

The results (3.27) and (3.28) allow us to identify the expression

$$\tilde{\rho}(p) = a^2(p) \frac{c^2 p^2 + (\hbar \omega_p - mc^2)^2}{p^2} \quad (3.35)$$

up to a due normalization, as the probability density in p -space, conjugate to the x -space probability defined in (3.5).

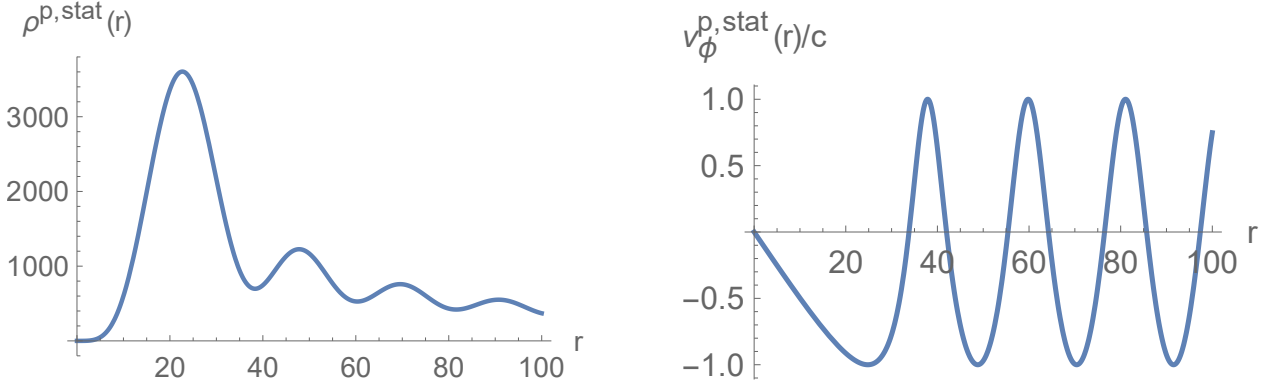


Figure 1: Stationary case: density $\rho^{p,\text{stat}}(r)$ and azimuthal velocity $v_\phi^{p,\text{stat}}(r)/c$ for $j = 5/2$, $p = 10^{-4}$ meV/c ($E = 100$ meV).

3.3 j - electrons in graphene

Let us denote free electrons in eigenstates of the total angular momentum with eigenvalue j as “ j -electrons”. Free electrons in mono-layer graphene [27] with energy less than $E_{\text{crit}} \approx 160$ meV obey approximatively a relativistic-like massless dispersion law $E \approx pc$, where p is the linear momentum and the “velocity of light”¹¹ $c \approx 10^6$ m s⁻¹. The dynamics of these electron is that of free massless particles in dimension three space-time with pseudo-spin 1/2 obeying the Dirac equation (3.2) with $m = 0$ [28]. Pseudo-spin is a chirality effect due to the peculiar crystalline structure of graphene and should not be confused with the usual spin. Nevertheless, since the wave function obeys the Dirac equation (3.2), the pseudo-spin adds itself to the orbital angular momentum yielding the conserved total angular momentum j (3.12) as explained in Subsection 3.2.

We will consider first stationary states and then states defined by Gaussian-like wave packets. Conventions and units used in the following are described in Appendix A.

3.3.1 Stationary states in graphene

As already shown in Subsection 3.2.1, the dBB trajectories associated to the stationary wave functions (3.21) are circles centred at the origin, travelled at a constant dBB velocity $v_\phi^{p,\text{stat}}$ which depends on the radius r according to (3.23). For $m = 0$, this velocity reads

$$v_\phi^{p,\text{stat}}(r) = 2c \frac{J_{j-1/2}(pr/\hbar)J_{j+1/2}(pr/\hbar)}{J_{j-1/2}^2(pr/\hbar) + J_{j+1/2}^2(pr/\hbar)}. \quad (3.36)$$

The dBB velocity value oscillates between $-c$ and c . A typical behaviour, as a function of the radius, of the probability density and of the dBB velocity, which depend on the energy $E = cp$ and on the angular momentum j , is shown in Fig. 1 for $j = 5/2$ and $E = 100$ meV. The most

¹¹This is the so-called critical velocity, which we will denote by c .

j	1/2	3/2	5/2	7/2	9/2	11/2	13/2	15/2	17/2
α_j	0	2.19	3.45	4.61	5.74	6.84	7.93	9.01	10.08

Table 1: Coefficients α_j of Eq. (3.38) as a function of the angular momentum j .

probable radius \hat{r}_j , is given by the position of the first maximum of the probability density $\rho^{p,\text{stat}}$ (3.22) (See Fig. 1), which for $m = 0$ reads

$$\rho^{p,\text{stat}}(r) = c^2 p^2 (J_{j-1/2}^2(pr/\hbar) + J_{j+1/2}^2(pr/\hbar)). \quad (3.37)$$

Since r appears in the combination pr/\hbar , the most probable radius \hat{r}_j may be written as a function of p :

$$\hat{r}_j(p) = \alpha_j \frac{\hbar}{p}, \quad (3.38)$$

the j -dependent coefficients α_j being shown in Table 1 for some values of j . These results can be taken as an approximation for the more realistic case of a wave packet with a very small energy width.

3.3.2 Gaussian wave packets in graphene

We turn now to the Gaussian wave functions defined by (3.24) and (3.25), which are normalizable. We shall denote by

$$\mathbf{x}_B(r_0, t) = (r_B(r_0, t), \phi_B(r_0, t)),$$

the (polar) coordinates of the dBB trajectory solution of the trajectory equation (2.7), fixed by the initial position

$$\mathbf{x}_B(r_0, 0) = (r_B(r_0, 0), \phi_B(r_0, 0)) = (r_0, 0). \quad (3.39)$$

We have made explicit, in our notation, the dependence on the trajectory parameter r_0 .

Figs. 2 and 3 show the most probable dBB trajectory $\mathbf{x}_B(\hat{r}_0, t)$ for a particular wave function's parametrization in which the energy dispersion is very small, *i.e.*, $\Sigma \ll p_0$. “Most probable” means that the initial particle's position parameter \hat{r}_0 is the value of the radial coordinate r which maximizes the initial probability density $\rho(r, 0)$. This value, equal to 22.7 nm in the present example¹², corresponds to the blue dot in Fig. 4a. Thus, the behaviour of this trajectory, shown by Figs. 2c or 3c in the (x, y) -plane, is very similar to the circular one shown in the corresponding stationary solution, but only up to a certain critical “decay time” τ_{obs} , approximately equal to 0.006 ns in this example. For later times the trajectory tends to a straight line, reproducing the expected classical behaviour. This is best observed in Figs. 2b or 3b which show the time behaviour of the azimuthal angle ϕ : the angular velocity

¹²This value is very near of the one corresponding to the stationary wave function with same $j = 5/2$ and p equal to the momentum parameter $p_0 = 10^{-4}$. Indeed, Eq. (3.38) together with Table 1 yield $\hat{r} = 22.6$.

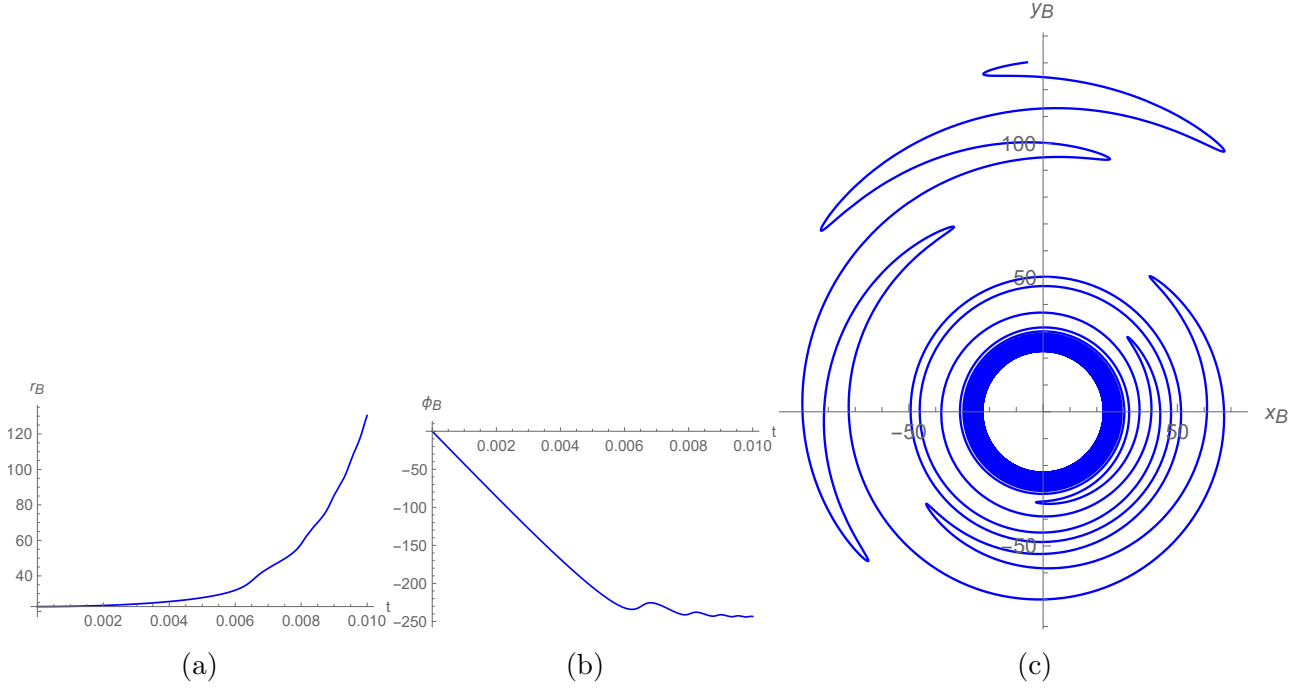


Figure 2: The most probable dBBS trajectory $\mathbf{x}_B(\hat{r}_0, t)$ for Gaussian wave packet parameters $j = 5/2$, $p_0 = 10^{-4}$ meV/c (Peak energy $E_0 = 100$ meV), and $\Sigma = 10^{-7}$ meV/c. This trajectory is fixed by the initial condition parameter $\hat{r}_0 = 22.7$. \hat{r}_0 is the position of the peak of the probability density ρ at $t = 0$ (the blue point in Fig. 4a.)

(a) Radial coordinate $r_B(\hat{r}_0, t)$.

(b) Azimuthal coordinate $\phi_B(\hat{r}_0, t)$.

(c) dBBS trajectory in the (x, y) plane for $0 \leq t \leq 0.010$ ns. The trajectory performs 38 loops before the critical time (decay time) $\tau \sim 0.006$ ns.

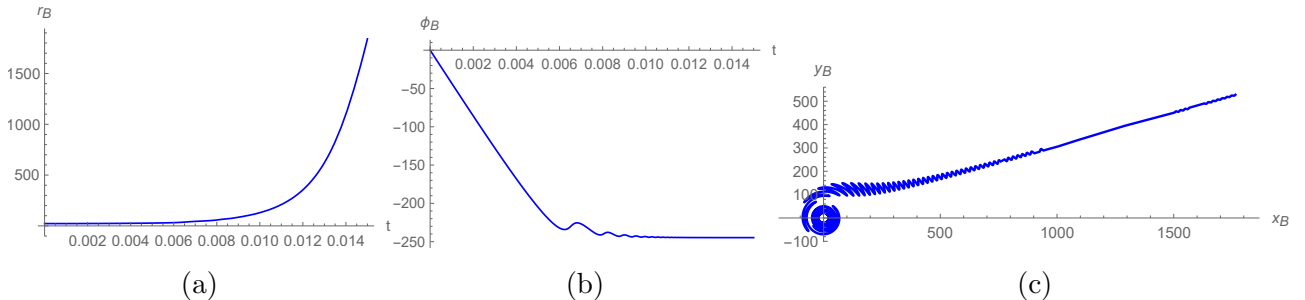


Figure 3: dBB trajectories for Gaussian wave packet: same parametrization as in Fig. 2, but with the larger time scale $0 \leq t \leq 0.015$ ns.

is almost constant until the time τ_{obs} , and almost vanishes thereafter. This decay time marks the transition from the almost circular regime to an almost straight-way, classical-like, regime.

A theoretical lower bound for the decay time τ may be computed from the quantum "time-energy uncertainty principle" [29]:

$$\tau \geq \tau_{\min} = \frac{\hbar}{2\Delta E}, \quad (3.40)$$

where ΔE is the quantum energy uncertainty given by (3.28). In our example, $\tau_{\min} = 0.00465$ ns: this is the order of magnitude of the observed decay time for the most probable trajectory, $\tau_{\text{obs}} \sim 0.006$ ns, and the uncertainty inequality (3.40) is obeyed.

A simple check of the quasi-classical nature of the trajectories for large times consists in comparing the quantum mean orbital angular momentum $\langle L \rangle = \hbar j$ given after Eq. (3.32), with the orbital momentum of a massless free classical particle of energy E running along a straight trajectory $r(t)$ defined by its position and velocity at some time t , given by

$$L_{\text{class}} = \frac{E}{c^2} r(t) v_\phi(t), \quad (3.41)$$

where $v_\phi(t)$ is its azimuthal velocity. Inserting for E in the latter expression the quantum mean energy $\langle E \rangle$ (3.29), and for $r(t)$, $v_\phi(t)$ the dBB trajectory function $r_B(t)$ and the corresponding azimuthal velocity, and equating it to the quantum expectation value $\langle L \rangle = \hbar j$, yields a value for L_{class} which, at a sufficiently large time, should tend to the value $\hbar j$ characterizing the considered wave function. For the particular case shown in Figs. 2 and 3, with $j = 5/2$ and a transition time $\tau_{\text{obs}} \sim 0.006$ ns, we have checked that the resulting value for L_{class} at the rather larger time $t = 0.030$ ns, indeed coincides with $\hbar j$ up to an error of the order of 10^{-5} . Such a concordance holds for the most probable or almost most probable trajectories, but tends to diminish for the less probable ones, *i.e.*, those for which the initial radial coordinate lies farther of the probability distribution's peak position shown, *e.g.*, in Fig. 4a.

Fig. 4 shows trajectories, calculated for the same wave function as for Figs. 2 and 3, for five initial radial positions.

Fig. 5 shows the time evolution of the absolute velocity $|\mathbf{v}|(r_0, t)$ for the state already exhibited in the figures above. $|\mathbf{v}|$ is shown for five dBB trajectories, characterized by their initial position parameters r_0 and colours as in Fig. 4. One observes that, for a each trajectory, the absolute velocity tends to the "velocity of light"'s value $c = 10^6$ nm/ns above a certain threshold. For example, for the blue trajectory, which corresponds to the initial radial position $r_0 = 22.7$, the threshold is at $t \sim 0.017$. It is a bit higher than the decay time τ (~ 0.006 ns here).

Table 2 displays, for certain values of the wave parameters p_0 , Σ and j , quantities of interest such as mean energy $\langle E \rangle$ (3.29), standard energy deviation ΔE (3.30), τ_{\min} (3.40), (which are usual quantum theory quantities), and also, specifically concerning the most probable dBB trajectory, its approximate observed decay time τ_{obs} , its L -radius r_L (3.33), its initial radial coordinate \hat{r}_0 (see (3.39)) which fixes it, and the number N_{loops} of closed loops it performs before passing to the straight-way regime.

One can make the following remarks about the items of Table 2.

1. The mean values $\langle E \rangle$, ΔE , hence τ_{\min} , do not depend on the quantum number j , which is

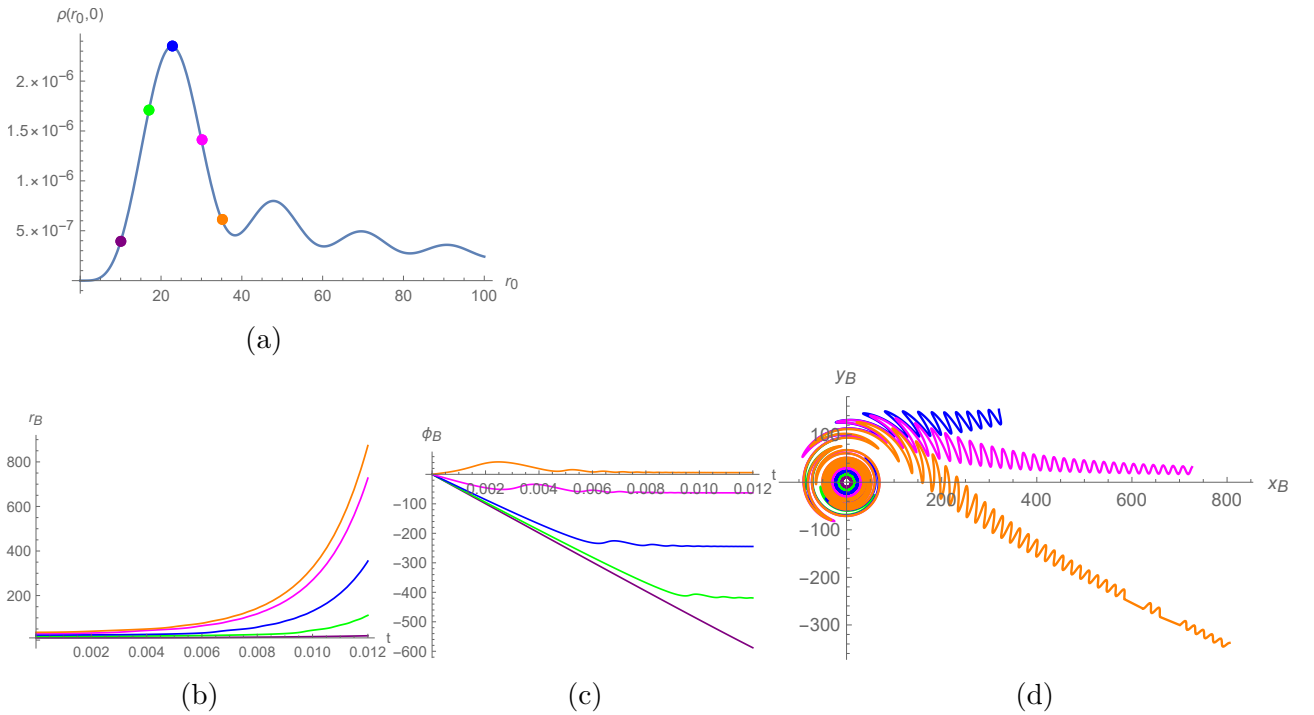


Figure 4: dBB trajectories for Gaussian wave packet: same parametrization as in Figs. 2 and 3, but with five trajectories corresponding to the initial radial positions $r_0 = 10, 17, 22.7, 30$ and 35 nm. The respective numbers of trajectory's closed loops are 93, 66, 38, 10 and 1. Their respective relative probabilities are proportional to the heights of the coloured dots in the sub-figure (a) showing the initial probability density $\rho(r_0, 0)$ as a function of the initial radial position r_0 .

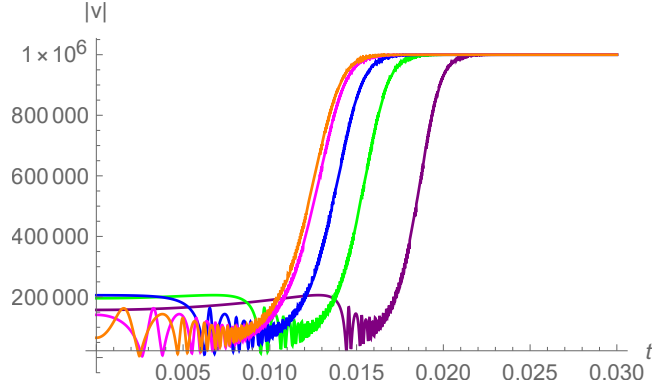


Figure 5: Absolute velocity $|v|$ as a function of t for the solutions shown in Figs. 2, 3 and 4. Colors correspond to the five different trajectories exhibited in Fig. 4.

$p_0(\frac{\text{meV}}{c})$	$\Sigma(\frac{\text{meV}}{c})$	$\langle E \rangle$ (meV)	ΔE (meV)	τ_{\min} (ns)	τ_{obs} (ns)	r_L (nm)	\hat{r}_0 (nm)	N_{loops}	j
10^{-5}	10^{-8}	10.0000	0.00707	0.0465	0.3	32.91	0	757	1/2
					0.06	164.6	227	39	5/2
					0.05	362.0	450	20	11/2
					0.05	3258.	3450	3	99/2
	10^{-6}	10.0995	0.704	0.000468	0.001	32.59	0	3	1/2
					–	162.9	220	< 1	5/2
					–	358.4	435	< 1	11/2
					–	3226.	3250	< 1	99/2
10^{-4}	10^{-7}	100.000	0.0707	0.00465	0.027	3.291	0	676	1/2
					0.006	16.46	22.7	39	5/2
					0.006	36.20	45.0	20	11/2
					0.005	325.8	345	3	99/2
	10^{-5}	100.995	7.04	0.0000468	0.0001	3.259	0	2	1/2
					–	16.29	22.0	< 1	5/2
					–	35.84	43.5	< 1	11/2
					–	322.6	325	< 1	99/2

Table 2: Mean energy $\langle E \rangle$, standard energy deviation ΔE , decay time lower bound τ_{\min} , observed decay time τ_{obs} , L -radius r_L , most probable initial radial coordinate \hat{r}_0 and number of trajectory loops N_{loops} for some values of the wave packet parameters p_0 , Σ and j . Trajectories concerned in columns 6 to 9 are the most probable ones.

obvious from the explicit expressions (3.29) and (3.30). $\langle E \rangle$ and ΔE tend towards their limit values (3.34) as the width Σ becomes narrower, as can be seen in the Table.

2. The observed decay time τ_{obs} seen in the behaviour of the azimuthal angle ϕ_{B} shown, *e.g.*, in Figs. 4c or 4d, depends on the specific trajectory: it diminishes when the value of the initial radial coordinate $r_{\text{B}}(r_0, 0) = r_0$ augments. On the other hand, its value does not depend sensibly on the quantum number j , as can be seen in the table.
3. Except for $j = 1/2$, the L -radius r_L (3.33) is near of the value of the initial radial coordinate \hat{r}_0 of the most probable trajectory. This is what can be expected for the nearly circular motion which takes place at times $t < \tau_{\text{obs}}$.
4. The number of revolutions also tends to decrease with increasing initial position r_0 , as shown in the example of Fig. 4, which shows five trajectories corresponding to five different initial radial positions.
5. The behaviours observed in these examples are generic, this being confirmed by all other cases we have numerically studied.

Concluding this subsection, an important observation can be made. Although the minimum value for the decay-time τ was inferred from the usual quantum theoretical uncertainty principle for time-energy (3.40), it appears difficult to interpret τ in this framework. But it looks quite natural in the dBB scheme, namely as a property of the dBB trajectories.

3.3.3 Times of flight

The dBB theory also offers a very natural way to define the time of flight of a particle which has followed a dBB trajectory $\mathbf{x}_{\text{B}}(\mathbf{x}_0, t)$ from its initial position \mathbf{x}_0 to some target, *e.g.*, consisting of a detector. In our case, one can think of a detector occupying a circle of radius R centered at the origin. This time of flight is then the solution $t_{\text{flight}}(R, r_0)$ of the equation

$$r_{\text{B}}(r_0, t_{\text{flight}}) - R = 0, \quad (3.42)$$

where $r_{\text{B}}(r_0, t)$ is the radial coordinate of the considered trajectory, characterized by its initial radial coordinate r_0 . In case the solution is not unique, one has to take the lowest one, corresponding to the first hit of the particle to the target [15, 16]. However, this precaution is not needed in all cases we have investigated, where $r_{\text{B}}(r_0, t)$ is a monotonically increasing function of t .

The empirically interesting quantity is the probability distribution $\Pi(\tau)$ in terms of the time of flight $t_{\text{flight}} = \tau$. It is given by the equation (9) of [15], which in our context takes the form:

$$\begin{aligned} \Pi(\tau) &= N2\pi \int_0^\infty dr_0 r_0 \rho(r_0, 0) \delta(t_{\text{flight}}(R, r_0) - \tau) \\ &= N2\pi r_0(R, \tau) \rho(r_0(R, \tau), 0) / |\partial_{r_0} t_{\text{flight}}(R, r_0(R, \tau))|, \end{aligned} \quad (3.43)$$

where $r_0(R, \tau)$ is the inverse of the time of flight function $t_{\text{flight}}(R, r_0)$, *i.e.*, the solution (unique, here) of (3.42) for r_0 in terms of R and $t_{\text{flight}} = \tau$. Recall that $\rho(r_0, 0)$ represents the probability

distribution for the trajectory defined by its initial radial coordinate r_0 . N is a normalization factor ensuring the normalization condition

$$\int_0^\infty d\tau \Pi(\tau) = 1. \quad (3.44)$$

If the probability flux through the detector's entry is always positive, which is the case in our examples¹³, an alternative expression for the probability distribution is given by [14]

$$\Pi_{\text{Flux}}(\tau) = N \int_{\Sigma} d\mathbf{s} \cdot \mathbf{j}(\mathbf{x}, \tau) \stackrel{\text{(here)}}{=} N 2\pi R j_r(R, \tau), \quad (3.45)$$

where \mathbf{j} is the probability flux and Σ the detector entry's surface. This result was proved in a scattering context by [14], and more generally, but in the one-dimensional case, by [32], and by [33] in the case of a spinless non-relativistic particle. We have checked numerically the equivalence of both formulae (3.43) and (3.45) in our specific situation for various parametrizations of the wave function. Figs. 6 and 7 show the time of flight as a function of the trajectory pa-

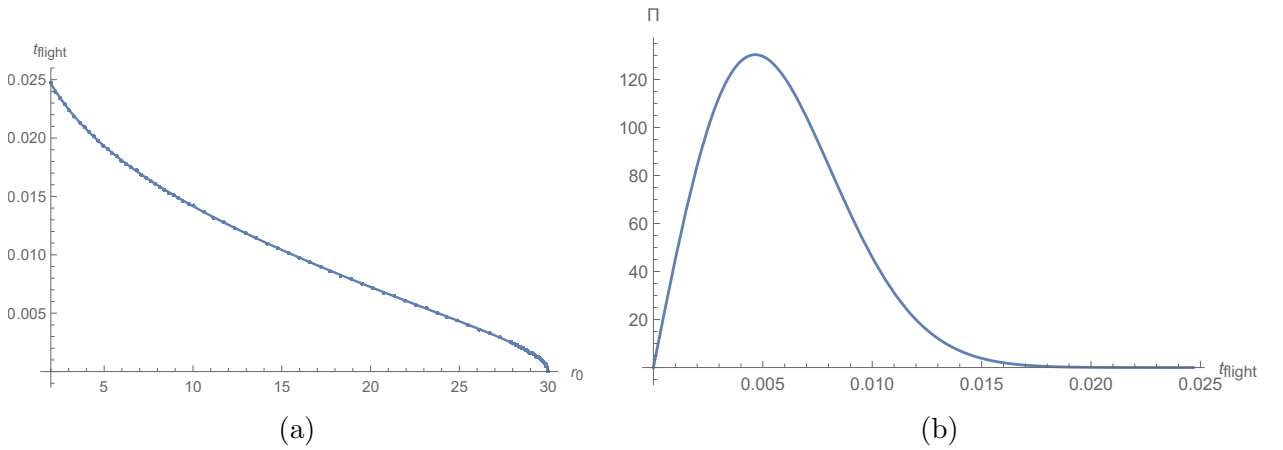


Figure 6: Times of flight t_{flight} solutions of (3.42) and values of their probability density $\Pi(t_{\text{flight}})$ (3.43) for the dBB trajectories shown in Fig. 4. The wave function parameters are the same as those in Figs. 2 to 5. The target is a circle centred at the origin, with radius $R = 30$ nm. The initial radial coordinate r_0 varies between 2 and 30 nm.

(a) Values of the time of flight for each dBB trajectory. The dots represent the numerically calculated values, and the continuous line an interpolation used for the calculation of the probability distribution.

(b) Values of the corresponding probability density. Use of Eq. (3.45) has been made.

parameter r_0 and the corresponding probability distribution (3.43) for a circular target of radius 30 and 500 nm, respectively.

¹³Examples where this is not the case are presented and discussed in [30, 15, 16, 31].

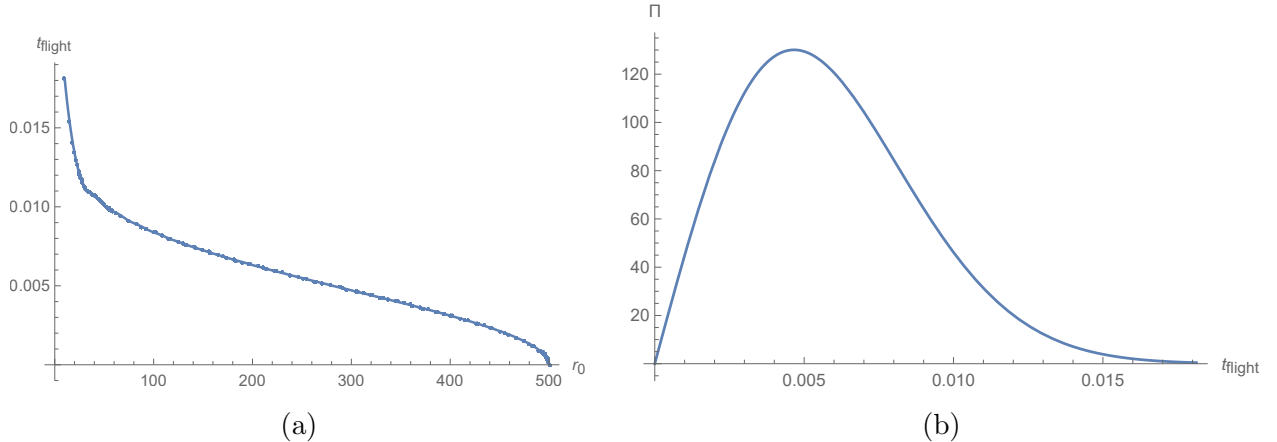


Figure 7: Same as Fig. 6, but with target’s radius $R = 500$ nm and initial radial coordinate r_0 in the interval 10 to 500 nm.

4 Conclusion

The trajectories predicted by the de Broglie-Bohm (dBB) quantum theory were calculated for the case of a guiding wave function being solution of the two-dimensional free Dirac equation, a solution constrained to be an eigenfunction of the total angular momentum operator relative to a given origin point of space. Numerical results have been provided for the case of massless particles with momentum-energy specifications corresponding to those of free electrons in mono-layer graphene.

The trajectories corresponding to stationary wave functions turn out to be circles travelled at a constant speed. For Gaussian-like wave packets, the trajectories begin as quasi circles of slowly increasing radius till a critical time at which they tend to straight lines approximating the behaviour expected for a classical free particle. This transition time decreases when the value of the initial radial coordinate which labels a particular trajectory increases, but appears to be insensible to the chosen value of the total angular momentum. It is worth noting that the transition time obtained in each example is of the order of magnitude of, but greater than, the lower bound given by the ”time-energy uncertainty principle”. Although the nature of this lower bound is of course purely quantum mechanical, a theory such as the dBB one appears necessary in order to interpret it. More, it is the use of the dBB theory which has allowed us to put this phenomenon in evidence.

Given a wave function, the possible times of arrival of the particle at some region have also been calculated as a function of its initial position for the same examples, taking profit of the objective reality of the trajectories in the dBB theory. The corresponding probability distribution of these arrival times has been calculated using the Das-Dürri formula (3.43) and also the probability flux formula (3.45). Both calculation’s results coincide, as can be expected from the equivalence’s proof given in [32] for the spin one-half particle in one-dimensional space

and by [33] for the non-relativistic spinless particle. Note that this equivalence holds if the flux on any target is always positive – which is true in our examples. The interest of this probability distribution is that it may in principle be measured in a given physical context such as, *e.g.*, the mono-layer graphene, after a suitable analysis of the experimental setting.

Acknowledgements

I would like to thank Siddhant Das for his reading of the manuscript, the indication of interesting references and valuable comments.

Appendices

A Notations and conventions

Units used in this paper are adapted to the physics of graphene. Length, time and energy are given in nm, ns and meV, respectively. The critical velocity and the Planck constant take the values

$$c = 10^6 \text{ nm ns}^{-1}, \quad \hbar = 6.5821 \times 10^{-4} \text{ meV ns.} \quad (\text{A.1})$$

Space-time coordinate are denoted by x^μ , $\mu = 0, 1, 2$, space coordinates by $\mathbf{x} = (x, y)$, or (r, ϕ) . Space-time metric is $\eta_{\mu\nu} = \text{diag}(1, -1, -1)$

Dirac matrices are chosen in terms of the Pauli matrices as

$$\gamma^0 = \sigma^z, \quad \gamma^1 = \gamma^0 \sigma^x, \quad \gamma^2 = \gamma^0 \sigma^y. \quad (\text{A.2})$$

The Dirac matrices $\alpha^i = \gamma^0 \gamma^i$ used in the non-relativistic formulation explicitly are

$$\alpha^1 = \sigma^x, \quad \alpha^2 = \sigma^y, \quad \beta = \sigma^z. \quad (\text{A.3})$$

B Some useful properties of the Bessel functions

The general solution of the Bessel equation [34]

$$z^2 f''(z) + z f'(z) + (z^2 - n^2) f(z) = 0, \quad (\text{B.1})$$

has the form

$$f(z) = C_1 J_n(z) + C_2 Y_n(z), \quad (\text{B.2})$$

where J_n and Y_n are the Bessel functions of the first [34], respectively second [34] kind, and C_1 , C_2 are two arbitrary complex constants. We shall restrict ourselves to an integer index n .

The asymptotic behaviours of the Bessel functions at the origin are given by

$$\begin{aligned} J_n(x) &\sim \frac{1}{n!} \left(\frac{x}{2}\right)^n && (0 < x \ll 1, n \geq 0), \\ Y_n(x) &\sim -\frac{(n-1)!}{\pi} \left(\frac{2}{x}\right)^n && (0 < x \ll 1, n \geq 1), \\ Y_0(x) &\sim \frac{2}{\pi} \log\left(\frac{x}{2}\right) && (0 < x \ll 1), \end{aligned} \tag{B.3}$$

and at infinity by

$$\begin{aligned} J_n(x) &\sim \sqrt{\frac{2}{\pi x}} \cos\left(x - \frac{(n + \frac{1}{2})\pi}{2}\right) && (x \gg 1, n \geq 0), \\ Y_n(x) &\sim \sqrt{\frac{2}{\pi x}} \sin\left(x - \frac{(n + \frac{1}{2})\pi}{2}\right) && (x \gg 1, n \geq 0). \end{aligned} \tag{B.4}$$

Functions with a negative index are related to those with a positive one by the identities

$$J_{-n}(z) = (-1)^n J_n(z), \quad Y_{-n}(z) = (-1)^n Y_n(z). \tag{B.5}$$

Under parity $z \rightarrow -z$, the function J_n transforms as

$$J_n(-z) = (-1)^n J_n(z). \tag{B.6}$$

An interesting orthogonality property is given by [34]

$$\int_0^R dr r J_n\left(\frac{z_{n,\alpha} r}{R}\right) J_n\left(\frac{z_{n,\beta} r}{R}\right) = \frac{R^2}{2} (J_{n+1}(z_{n,\alpha}))^2 \delta_{\alpha\beta}, \tag{B.7}$$

for $n \geq 0$, where $z_{n,\alpha}$ is the α^{th} positive zero of the Bessel function $J_n(z)$ [35]. Moreover, any function $f(r)$ defined in the interval $0 \leq r \leq R$ with bounded variation and vanishing at the end point $r = R$ can be represented as a ‘‘Fourier Bessel series’’ [36] as

$$f(r) = \sum_{\alpha=1}^{\infty} c_{\alpha} J_n\left(\frac{z_{n,\alpha} r}{R}\right), \tag{B.8}$$

for any $n \geq 0$. The coefficients c_{α} can be calculated using the orthogonality formula (B.7).

Declarations

No funds, grants, or other support was received.

The author has no relevant financial or non-financial interests to disclose.

The Mathematica notebook file relevant for the numerical calculations made in this research may be required at author’s e-mail: *opigu@yaho.com*.

References

- [1] Max Planck, “Ueber das Gesetz der Energieverteilung im Normalspectrum” (English translation), *Annalen der Physik* 4 (1901) 553.
- [2] Niels Bohr, “On the Constitution of Atoms and Molecules”, *Philos. Mag.* 26 (1913) 1 and 476.
- [3] Albert Einstein, “Concerning an Heuristic Point of View Toward the Emission and Transformation of Light”, *Annalen der Physik* 17 (1905) 132.
- [4] Louis de Broglie, “Recherches sur la théorie des quanta”, Thesis (Paris), 1924;
Louis de Broglie, *Ann. Phys. (Paris)* 3, 22 (1925). Reprint in *Ann. Found. Louis de Broglie* 17 (1992) p. 22;
Louis De Broglie, “La mécanique ondulatoire et la structure atomique de la matière et du rayonnement”, *J. Phys. Radium* 8 (1927) 225, DOI 10.1051/jphysrad:0192700805022500.
- [5] Erwin Schrödinger, “Quantisierung als Eigenwertproblem”, *Annalen der Physik* 79 (1926), 361, *Annalen der Physik* 79 (1926) 489, *Annalen der Physik* 80 (1926) 437, *Annalen der Physik* 81 (1926) 109.
- [6] Werner Heisenberg, “Über quantentheoretische Umdeutung kinematischer und mechanischer Beziehungen”, *Z. Phys.* 33 (1925) 879.
- [7] Paul A.M. Dirac, “The quantum theory of the electron”, *Proc. R. Soc. A* 117 (1928) 610 and 118 (1928) 351.
- [8] Niels Bohr, “The Quantum Postulate and the Recent Development of Atomic Theory”, *Supplement to "Nature"* April 14 (1928) 580;
Werner Heisenberg, “Physics and Philosophy”, Harper, New York (1958),
- [9] Hugh Everett, “Relative State Formulation of Quantum Mechanics”, *Rev. Mod. Phys.* 29 (1957) 454.
- [10] Carlo Rovelli, “Relational quantum mechanics”,
Int. J. Theor. Phys. 35 (1996) 1637 e-Print: quant-ph/9609002 [quant-ph];
Andrea Di Biagio and Carlo Rovelli, “Stable Facts, Relative Facts”,
Found. Phys. (2021) 51:30.
- [11] David Bohm, “A Suggested interpretation of the quantum theory in terms of hidden variables 1, 2.”, *Phys. Rev.* 85 (1952) 166, 180.
- [12] D. Bohm and B.J. Hiley, ”The Undivided Universe”, Routledge, London and New York (1995).
- [13] John S. Bell, “Speakable and Unspeakable in Quantum Mechanics”, *Cambridge University Press, New York* (2010).

- [14] M. Daumer, D. Dürr, S. Goldstein and N. Zanghi, “On the Quantum Probability Flux Through Surfaces”, *J. Stat. Phys.* 88 (1997) 967.
- [15] Siddhant Das and Detlef Dürr, ”Arrival time distributions of spin-1/2 particles, *Nature Scient. Rep.* 9 (2019) 2242.
- [16] Siddhant Das, Markus Nöth and Detlef Dürr, “Exotic arrival times of spin-1/2 particles I - An analytical treatment”, *Phys. Rev.* A99 (2019) 052124.
- [17] Peter R. Holland, “The quantum theory of motion”, Revised ed., Cambridge University Press (1995).
- [18] Detlef Dürr, Sheldon Goldstein, Travis Norsen, Ward Struyve and Nino Zanghi, “Can Bohmian mechanics be made relativistic?” *Proc. R. Soc. A* 470 (2013) 20130699
- [19] Roderich Tumulka, “On Bohmian Mechanics, Particle Creation, and Relativistic Space-Time: Happy 100th Birthday, David Bohm!”, *Entropy* 20 (2018) 462.
- [20] Dario Bressanini and Alessandro Ponti, “Angular Momentum and the Two-Dimensional Free Particle”, *J. Chem. Educ.* 75 (1998) 916.
- [21] Wolfram Research, Inc., Mathematica, Champaign, IL.
- [22] Abraham Pais, “On Spinors in n Dimensions”, *J. Math. Phys.* 3 (1962) 1135; doi: 10.1063/1.1703856.
- [23] D. Dürr D., S. Goldstein and N. Zanghi, “Quantum equilibrium and the origin of absolute uncertainty”, *J. Stat. Phys.* 67 (1992) 843.
- [24] P.R. Holland, “The Dirac equation in the de Broglie-Bohm theory of motion”, *Found. Phys.* 22 (1992) 1287.
- [25] The Wolfram Functions Site,
<https://functions.wolfram.com/Bessel-TypeFunctions/BesselJ/21/02/02/>
- [26] WolframMathWorld,
<https://functions.wolfram.com/GammaBetaErf/Erf/>
- [27] Mikhail I. Katsnelson, “The Physics of Graphene” 2nd Edition, Cambridge University Press, Cambridge (2020).
- [28] S. Das Sarma, Shaffique Adam, E. H. Hwang and Enrico Rossi, “Electronic transport in two-dimensional graphene”, *Rev. Mod. Phys.* 83 (2011) 407, e-Print: arXiv:1003.4731 (cond-mat.mtrl-sci).
- [29] Albert Messiah, “Quantum Mechanics”, Vol. 1, Section VIII-13, Dover Publications, New York (2014) (English translation of “Mécanique Quantique”, Dunod, Paris, (1962)).
- [30] Detlef Dürr and Stefan Teufel, ‘Bohmian Mechanics’, Chap 16, Springer, Heidelberg (2009).

- [31] Siddhant Das, “Relativistic electron wave packets featuring quantum backflow”, *e-print* arXiv:2112.13180.
- [32] C. Richard Leavens, “Bohm Trajectory Approach to Timing Electrons”, p. 129 of “Time in Quantum Mechanics - Vol.1”, 2^d Ed., J.G. Muga, R. Sala Mayato, Í.L. Egusquiza (Eds.), *Lecture Notes in Physics* 734, Springer, Heidelberg, 2008.
- [33] Siddhant Das and Markus Nöth, Times of arrival and gauge invariance, *Proc. R. Soc. A* 477 (2021) 20210101, <https://doi.org/10.1098/rspa.2021.0101>.
- [34] WolframMathWorld, “Bessel function”,
<https://mathworld.wolfram.com/topics/BesselFunctions.html>.
- [35] WolframMathWorld,
<https://mathworld.wolfram.com/BesselFunctionZeros.html>
- [36] Eric W. Weisstein, “Fourier-Bessel Series.” From MathWorld—A Wolfram Web Resource.
<https://mathworld.wolfram.com/Fourier-BesselSeries.html>